Journal of Materials Processing Technology 214 (2014) 445–455

Contents lists available at ScienceDirect

Journal of Materials Processing Technology

journal homepage: www.elsevier.com/locate/jmatprotec

Multiple instability-constrained tube bending limits

H. Li[a], H. Yang[a,*], Z.Y. Zhang[a], G.J. Li[b], N. Liu[a], T. Welo[c]

[a] State Key Laboratory of Solidification Processing, Northwestern Polytechnical University, Xi'an 710072, China
[b] Chengdu Aircraft Industry (Group) Corporation Ltd., Chengdu 610092, China
[c] Department of Engineering Design and Materials, Norwegian University of Science and Technology, Trondheim, Norway

ARTICLE INFO

Article history:
Received 28 January 2013
Received in revised form
23 September 2013
Accepted 28 September 2013
Available online 7 October 2013

Keywords:
Forming limit
Tube bending
Instabilities
Formability

ABSTRACT

Understanding the bending limits is critical to extract the forming potential and to achieve precision tube bending. The most challenging task is the development of the tube bending limits in the presence of unequal deformation induced multiple instabilities and multi-factor coupling effects. Using analytical and 3D-FE methods as well as experiments, a comprehensive map of the tube bending limits during rotary draw bending is provided under a wide range of tube sizes, material types and processing parameters. The major results show: (1) For each instability, the intrinsic factors (tube geometrical parameters, D and t, and mechanical properties, m) dependent bending limits are clarified, and evident interactive or even conflicting effects are observed. (2) Under mandrel bending, the significant effects of the intrinsic factors on the wrinkling limit are reduced, the neglected effects of D/t on the thinning limit are magnified; the significant influences of D/t on the flattening limit even become contrary, and the effects of m on wrinkling and thinning limit are opposite to that on the flattening limit. (3) Taking D/t as the basic design parameter, a conceptual multiple defect-constrained bending limit diagram (BLD) is constructed, and a knowledge-based stepwise method for determining and improving tube bending limits is proposed, considering coupling effects of multiple forming parameters, e.g., intrinsic factors, tooling/processing parameters and uncertainties. (4) The method is experimentally verified by several practical bending scenarios for different kinds of tubular materials with extreme size.

1. Introduction

As one type of lightweight components for 'blood transfusion' or structural weight-bearing, bent tubular parts have been increasingly used in applications requiring diverse geometrical specifications and different quality tolerances for various industries, such as the aerospace, automobile, shipbuilding, energy and health care ones. Knowledge regarding the bending limit, i.e., the maximum deformation a tube can experience without bending failures, is a crucial issue in the exploration of the forming potential and the optimal design for precision tube bending (SAE Aerospace, 2004). However, upon bending, unequal tension and compression deformation inevitably occurs (shown in Fig. 1) at the extrados and intrados of the bend tube. Several inelastic instabilities may be induced, such as wrinkling, flattening (distortion) and over-thinning or even necking (cracking). Thus, different mechanisms causing these defects may exert coupling or even conflicting effects of various forming parameters on tube bending limits. A method for reducing one type of instabilities may probably cause another one to be much more severe (Li et al., 2007a,b). The co-existence of multiple defects and their interactions make determination and improvement of tube bending limit a challenge.

Currently, to improve the performance, the precision bending of advanced tubular materials with extreme geometrical specifications is urgently needed in practice. The materials such as Ti-alloy, Mg-alloy, and high-strength steel tubes are generally hard to deform with low ductility. The extreme structures are characterized by large diameters ($D > 40$ mm), small diameters ($D < 10$ mm), thin wall thicknesses ($D/t > 30$ mm), small bending radii ($R_d/D < 3$) and large bending angles ($\varphi > 90°$). Bending tubes with these features may undergo larger/unequal strain conditions and thus encounter higher risks of multiple defects co-occurring. Meanwhile, as shown in Table 1, the requirements for the bending quality with respect to the maximum wrinkling height, δ_w, thinning, δ_t, and flattening, δ_D, have become much more strict and diverse in many industries (SAE Aerospace, 2007). This sharpens the difficulty in determining and improving the bending limits of tubes. Due to lack of knowledge on multiple defects-constrained bendability, for the bent tubes with small R_d, the welding of several pieces of deep drawn parts has to be used, which not only causes high cost and weight, but also reduces the fluid

* Corresponding author. Tel.: +86 29 88495632; fax: +86 29 88495632.
E-mail addresses: liheng@nwpu.edu.cn, lhseeplan@gmail.com (H. Li), yanghe@nwpu.edu.cn (H. Yang).

0924-0136/$ – see front matter © 2013 Elsevier B.V. All rights reserved.
http://dx.doi.org/10.1016/j.jmatprotec.2013.09.027

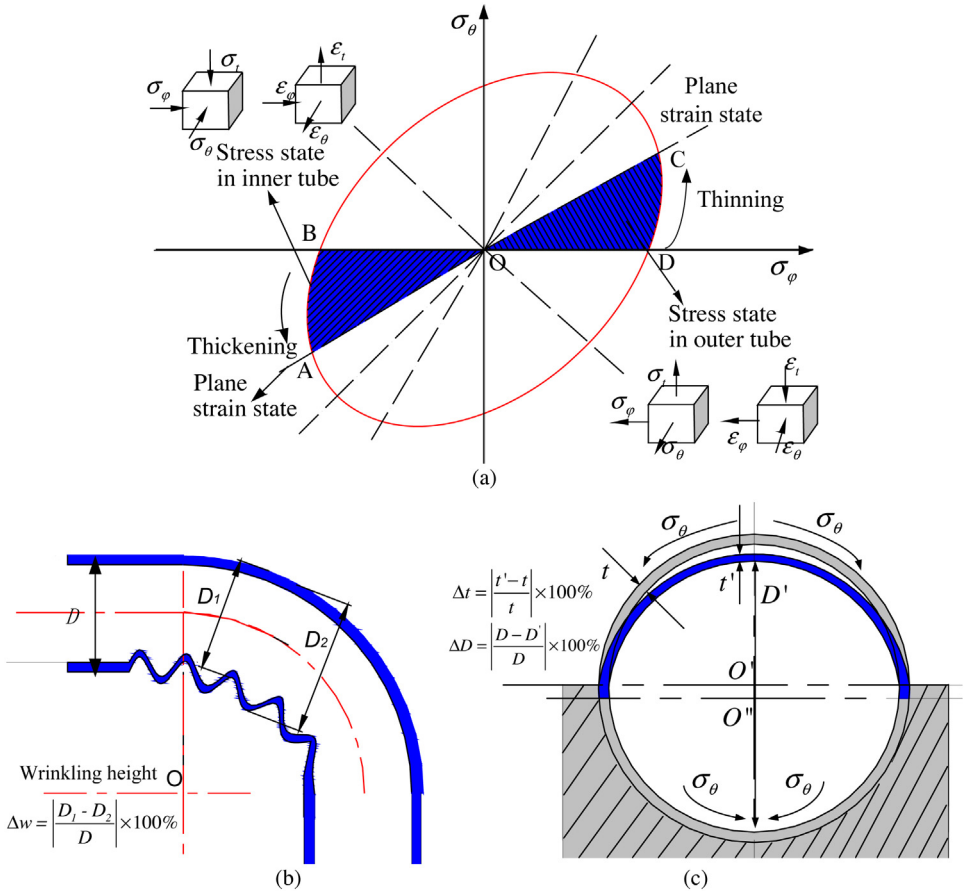

Fig. 1. Unequal stress/strain distributions and multiple instabilities in tube bending: (a) stress/strain states; (b) wrinkling; (c) thinning and flattening.

flow volume and flow rate. Thus, good insight into the multiple instability-constrained bending limits of tubes should be obtained to find a logical way to improve the bending formability in the presence of the coupling effects of multiple factors, e.g., intrinsic factors (tube geometrical parameters, D and t, and mechanical properties, m), tooling/processing parameters and uncertainties in bending.

Great efforts have been taken to explore the formability of various materials using analytical, experimental or numerical approaches. The bending limits of tubular materials were extensively investigated under different bending operations. However, few reports considered multiple bending instabilities and the coupling effects of the various forming parameters to investigate multiple instability-related limits. Zeng and Li (2002) experimentally achieved difficult push bending of an Al-alloy tube with R_d equal to D using reasonable internal pressure and lubricant conditions. Goodarzi et al. (2005) experimentally proved that shear bending can produce Al-alloy bent tubes with small R_d via combining shear and bending modes. Using the minimum energy principle, Wang and Cao (2001) analytically calculated the wrinkling limit (minimum R_d without wrinkling) in tube bending. By introducing a new wrinkling wave function, Yang and Lin (2004) analytically obtained the effects of material properties on the wrinkling limit. With respect to thinning, Khodayari (2008) experimentally and analytically established the bending limit curve (BLC) of tube in Rotary Draw Bending (RDB) for various steel tubes and verified that the BLC provided more accurate prediction of the thinning limit than the standard FLC (forming limit diagram). Okude et al. (2012) showed that the usage of a wiper die and axial tension can improve the wrinkling limit of a square section tube in RDB. With respect to flattening, Lee et al. (2003) studied the bending limit of a square Al-alloy tube in rubber pad bending via experiments and FE simulation. Regarding a non-dimensional shape degradation factor, Lee et al. (2005) numerically obtained a hoop-buckle limit of oval tube bending. The mandrel roles in preventing the wrinkling and flattening of Al-alloy tubes and copper tubes in RDB were studied by Li et al. (2007a,b). Regarding thinning and flattening, Wu et al. (2008) explored the effects of temperature, bending velocity and grain size on the bendability of Mg-alloy AM30 tubes. For mandrel-free RDB (without internal supports) of small diameter tubes, the relationship between tube geometrical variables was correlated with cross-ovalization by Mentella and Strano (2012). These studies provide beneficial understanding on bending limits of various types of tubes. While, since the interactions between multiple instabilities and the coupling effects of overall parameters on these defects have not yet been identified, how to determine and improve

Table 1
Diverse bending tolerances with respect to the three major defects (SAE Aerospace, 2007).

Working pressure	Tube materials	Maximum wrinkling height δ_w (%)	Thinning δ_t (%)	Flattening δ_D (%)
Under 3.45 MPa	Al-alloy, steel	2	30	10
	Ti-alloy	2	30	5
Over 3.45 MPa	Al-alloy, steel	1	25	5
	Ti-alloy	No visible wrinkling	25	3

the multiple instability-constrained bending limits are hence still not available. The 'trial-and-error' method is still used for special case, combined with the technician's experience.

For the most universal bending, RDB, this study attempts to develop a comprehensive map of tube bending limits considering a wide range of tube sizes and material types. First, the index for fully identifying the multiple defect-constrained bending limits of tubes is clarified. Then, using three analytical models for prediction of wrinkling, thinning and flattening, the intrinsic factors dependent limits are compared for each instability. Third, combining 3D-FE model with the experiments, the coupling effects of the intrinsic factors on the tube bending limits are analyzed under contact conditions, and a multiple instability-constrained bending limit diagram (BLD) against the basic design parameters, D/t, is constructed. Finally, considering the coupling effects of tooling/processing parameters and uncertainties, a method to determine and improve the bending limits of tubes is proposed and evaluated by several practical scenarios.

2. Research methodology

2.1. Experimental procedure

Three kinds of benders, W21YPC-63, 159 and 219 mm, are available to validate the theoretical predictions. As shown in Fig. 2(a), three basic tools are used to realize mandrel-free tube bending: a bend die, a clamp die and a pressure die. The tube is clamped against the bend die by the clamp die and the pressure die. Then, the clamp die and bend die rotate simultaneously to draw the tube past the tangent point and rotate along the bend die groove for the desired R_d and φ. For difficult bending conditions with strict quality tolerance, the mandrel (with multiple flexible balls) and wiper die are indispensable to improve the bending quality. The process, using complete set of tools, is named mandrel bending as shown in Fig. 2(b).

Different types of tubular materials and specifications are employed. Table 2 shows the mechanical properties of the tube materials, as measured by the uniaxial tension test, in which the arc specimen or tubular section specimen was directly cut out from the tube along the longitudinal direction as shown in Fig. 3. The bold values are the default ones for the following computations without special declaration. Both the longitudinal and vertical extensometers are used for accurate strain recording and calculation of normal anisotropy exponent R. According to the volume conservation theory, the values of R can be calculated by Eq. (1) or Eq. (2) for the tubular section specimen and arc specimen, respectively.

$$R = \frac{\varepsilon_b}{\varepsilon_t} = \frac{\ln((D_1 + d_1)/(D + d))}{\ln(t_1/t)} \tag{1}$$

where D and t are the initial outer diameter and wall thickness of the tube, D_1 and t_1 are the transient outer diameter and wall thickness of the tube.

$$R = \frac{\varepsilon_b}{\varepsilon_t} = \frac{\varepsilon_b}{-(\varepsilon_l + \varepsilon_b)} = -\frac{\ln(b_1/b_0)}{(\ln(l_1/l_0) + \ln(b_1/b_0))} \tag{2}$$

where l_0 and b_0 are the initial length and width of specimen gauge, b_1 and l_1 are the transient width and length of the arc specimen gauge.

2.2. Theoretical models for prediction of tube bending limits

2.2.1. Analytical models to predict tube bending limits

Via the deformation theory of plasticity and the minimum energy principle, three analytical models are derived to predict the three instabilities related bending limits of tubes. The Hill'1948 anisotropic yield model and the Swift strain hardening function $\bar{\sigma} = K(\bar{\varepsilon} + \varepsilon_0)^n$ are used. The spatial stress/strain distributions of a tube during bending are formulated in supplementary file.

- Wrinkling limit prediction

Under local compressive stresses, the deformation energy required for wrinkling initialization is the lowest among all possible deformation phenomena under given bending conditions. This minimum-energy prediction criterion is used to indicate the wrinkling onset in tube bending, as shown in Eq. (3) (Li et al., 2009). The wrinkling ratio, I_w, is used to indicate the wrinkling tendency, i.e., larger I_w represents a higher risk of wrinkling, and when I_w equals 1.0, wrinkling occurs. The equation can be used to calculate the wrinkling limit of tubular materials.

$$I_w = \frac{T(T_1 + T_2)}{W_{min}(W_1 + W_2)} \tag{3}$$

where W_{min} is the minimum wrinkling energy, W_1 the wrinkling energy for bending curves of tube, W_2 the wrinkling energy for straight regions of tube, T the external force energy for stable bending deformation, T_1 the external energy for the curved region of tube, and T_2 the external energy for the straight portion. The formulation of each energy value can be found in the literature (Li et al., 2009).

- Thinning limit prediction

Bending induced tensile stress at the bent tube extrados makes wall thinning an inevitable phenomenon (shown in Fig. 1). While, over-thinning should be strictly avoided. The maximum degree of wall thinning, Δt, can be obtained by the thickness strain in supplementary file. With respect to the allowable maximum thinning degree, δ_t, the thinning limit can be calculated using Eq. (4):

$$\Delta t = (1 - e^{\varepsilon_t}) \times 100\% = \left(1 - \left(\frac{R_d + c \cdot r_0}{\rho}\right)^{-(1/1+r)}\right) \times 100\% \le \delta_t \tag{4}$$

where c the flattening coefficient, expressed as $c = (1 - Y/D)$, Y the reduction in tube diameter after bending, regarded as the clearance between the tube and the mandrel in mandrel bending, r the ratio of hoop strain to thickness strain, similar to the definition of the normal anisotropy coefficient, R (the Lankford coefficient), an experimentally measured value of approximately 1/3, and ρ is the neutral axial (NA) radius.

- Flattening limit prediction

Subjected to the resultant force of tension and compression stress, as shown in Fig. 1, flattening is another inevitable phenomenon during bending. Flattening is governed by tension stresses, which forces the stressed regions of the bent tube toward the neutral region of the tube cross-section. The cross-section deformation of a tube in RDB occurs mainly at the outside region of the tube because the inner side of the tube is rigidly supported by the bending die groove. Applying the force equilibrium equations and the minimum energy principle, with respect to the allowable maximum degree of flattening, δ_D, the flattening limit can be obtained by solving Eq. (5) (Paulsen and Welo, 2003):

$$\Delta D = \frac{D - D'}{D} \times 100\% = \frac{9}{128}\frac{D^4}{R_d^2 t^2}\left(\frac{2R_d b}{D}\right)^n \left\{\frac{\sqrt{\pi}}{(n-3)}\frac{\Gamma(1-(n/2))}{\Gamma(1/2-(n/2))} - \frac{n}{(n-2)(n-4)}\right\} \le \delta_D \tag{5}$$

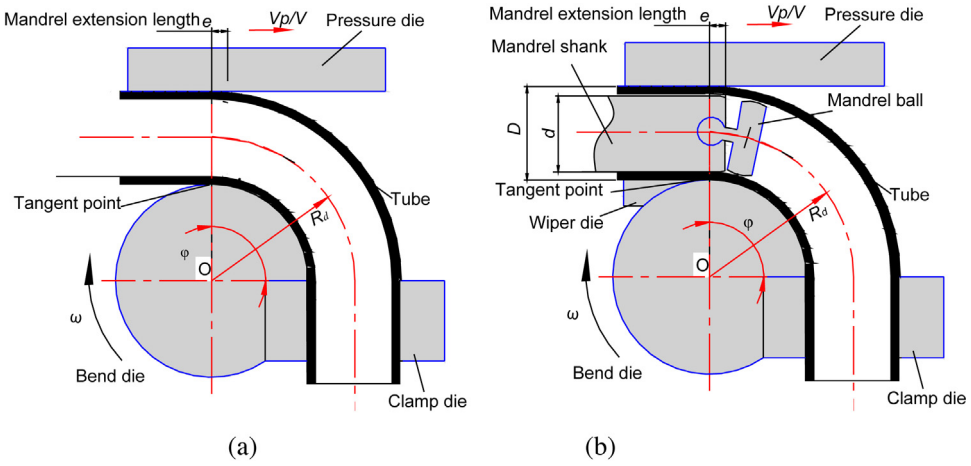

Fig. 2. Forming principle for tube during RDB: (a) mandrel-free bending; (b) mandrel bending.

Table 2
Mechanical properties of tubular materials.

Materials and specifications	5052-O 50 × 1.5	6061-O 38 × 1.0	6061-T4 9.52 × 0.51	1Cr18Ni9Ti 38 × 1.0	Ti-3Al-2.5V 6.35 × 0.4
Young's modulus, E (GPa)	**55**	36.6	58.7	200	109.7
Fracture elongation, δ (%)	**22**	26.5	25.7	60.3	13.0
Initial yield stress, $\sigma_{0.2}$ (MPa)	**90**	55	164	213	780.0
Strength coefficient, K (MPa)	**431**	226.1	527.6	1591	1236.5
Strain hardening exponent, n	**0.262**	0.283	0.276	0.54	0.078
Material constant, ε_0	**0.000**	0.000	0.000	0.000	0.0066
Normal anisotropy exponent, R	**0.55**	0.721	0.767	0.94	3.90

where Γ is the Gamma function and b the plastic offset strain, expressed as $(\sigma_0/K)^{1/n}$.

2.2.2. 3D-FE models considering multi-die constraints

Considering the contact conditions of multiple bending tools, the 3D-FE models of the entire RDB process (bending, ball retraction and unloading) are developed (shown in Fig. 4) to predict the multiple defects using the FE platform ABAQUS. An explicit algorithm is used to model the tube bending and ball retracting operations, while an implicit one is used for the springback. The detailed FE modeling can be found in the literature (Li et al., 2007a,b). Here, only the major modeling characteristics are presented.

- Modeling the material

When D/t of the tube exceeds 20, the tube is meshed with a four-node, doubly curved, thin shell S4R; When D/t of the tube is smaller than 20, the tube is discretized using a 3D linear reduction integration continuum element, C3D8R, with eight nodes, using enhanced hourglass control. The four-node bilinear rigid quadrilateral element, R3D4, is used to model the rigid bending tools. For the solid model, four integration points, used with the Simpson integration rule, are used through the tube wall thickness. Both the element size and the mass scaling factor are obtained by the convergence analysis to ensure a good tradeoff between numerical accuracy and stability.

- Modeling contact conditions

The boundary constraints are applied using two approaches to achieve realistic loading of RDB: displacement/rotate and velocity/angular. Table 3 shows the detailed contact conditions. The Coulomb friction model, $\tau = \mu p$, where τ is the frictional shear force, μ is the coefficient of friction (CoF) and p is the pressure force on the

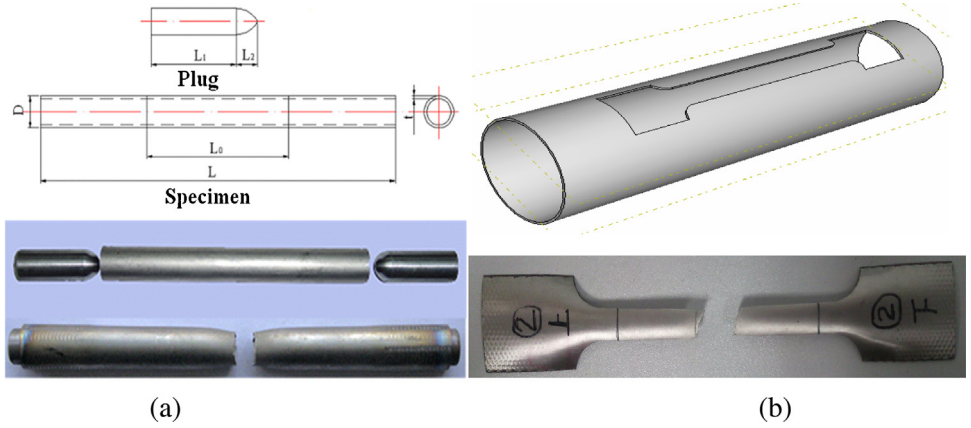

Fig. 3. Specimens for uniaxial tension tests: (a) tubular section specimen; (b) arc specimen.

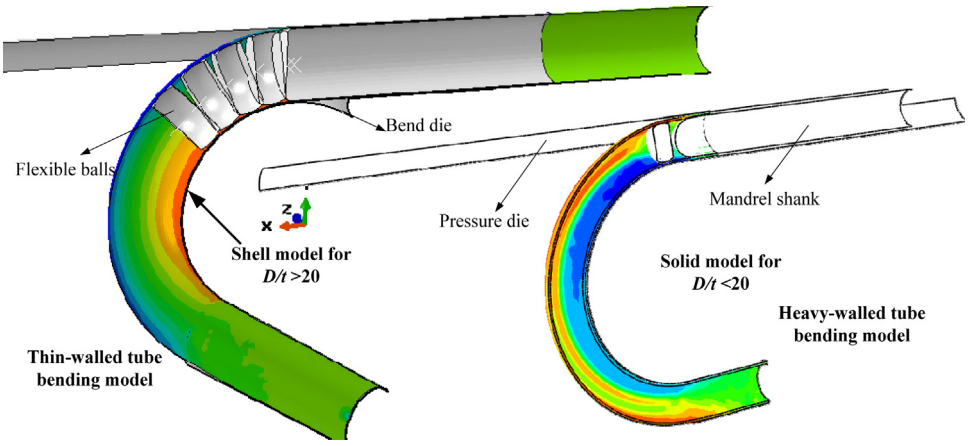

Fig. 4. 3D-FE models of tube bending, considering dynamic contact conditions.

Table 3
Friction conditions at various contact interfaces.

	Contact interface	CoF	Formulation of constraints	Lubricant conditions
1	Tube-wiper die	0.05	Kinematic method-finite sliding	Lubricated
2	Tube-pressure die	0.25	Kinematic method-finite sliding	DF (dry friction)
3	Tube-clamp die	0.6 (Rough)	Kinematic method-small sliding	Tough DF
4	Tube-bend die	0.1	Kinematic method-finite sliding	DF
5	Tube-mandrel	0.05	Kinematic method-finite sliding	Lubricated
6	Tube-flexible balls	0.05	Penalty method-finite sliding	Lubricated

contact surface, is used to represent the friction behavior between the tube and the die. The CoFs in Table 3 were the feasible values for tube bending deformation. For bending of different types of tubular materials, the different tribological conditions such as tool materials, surface roughness and lubricants, are designed to ensure the above reasonable CoFs on different contact interfaces. The friction behaviors under different tribological conditions can be measured and estimated by the simulative twist compression test (TCT) (Yang et al., 2010).

2.3. Evaluation of theoretical prediction models

The theoretical predictions are validated by the experiments as shown in Fig. 5. A 5052-O Al-alloy tube with bending angle of 90° is focused.

Fig. 5(a) shows the comparison of the analytically obtained wrinkling limits with the experimental results. All the predictions capture the features of higher wrinkling risk with larger D/t. Without considering the local wrinkling in RDB, the predictions by Wang and Cao (2001) are closer to the experimental results of pure bending (Corona et al., 2006), in which a four-point bending device was used. Compared with the analytical predictions of Yang and Lin (2004), the current analytical predictions of the wrinkling limits are closer to the experimental results for mandrel-free bending. Fig. 5(b) shows the comparison of the analytically predicted flattening of bent tubes with the experimental results of pure bending (Kyriakides and Ju, 1992). The current analytical predictions can accurately reproduce the flattening under different R_d, i.e., the increasing tendency to flatten with larger D/t. Since the wrinkling and distortion occur under mandrel-free bending, the thinning cannot be accurately measured and not compared with the analytical results. While, Fig. 5(c) shows that the analytical predictions of thinning also captures the feature of smaller thinning with larger D/t.

The comparisons of the 3D-FE results with the experimental ones are conducted. First, the mandrel diameter d is deliberately reduced to induce wrinkling. Then, the mandrel is removed to induce severe cross-section distortion. Last, two experiments of 50 mm × 1 mm × 75 mm and 50 mm × 1 mm × 100 mm are conducted for quantitative comparisons. e is 6.5 mm, and 2 flexible balls are used. Fig. 5(a) and (b) shows that the wrinkling location and shape as well as the distortion can be captured by the 3D-FE models. Fig. 5(c) shows that the maximum difference between the numerical and experimental results is less than 5%.

It is thought that 3D-FE models can accurately predict the bending behaviors in the case of rigid supports. However, because of the coupling effects of the contact conditions, the intrinsic relationships between the instabilities and the basic parameters (R_d, φ, D, t, and m) cannot be explicitly obtained by 3D-FE simulation. By contrast, despite of the limitation of various assumptions and the lack of inclusion of the contact conditions, the effect mechanisms of the intrinsic parameters on the three instabilities can be directly provided by the analytical models.

3. Results and discussion

Using the above theoretical models, regarding the three major instabilities, the tube bending limits are comprehensively addressed by changing various conditions, such as R_d, φ, D, t, m, tooling/processing parameters and uncertainties. The analytical models are used to provide direct insight into the effect mechanism of the intrinsic factors (R_d, φ, D, t, m), and the 3D-FE models are used to identify the coupling effects of the tooling/processing factors on bending limits under mandrel bending.

3.1. Dual indexes for multi-defect constrained bending limits

As shown in Eq. (6), the bending limits rely on the I_w, I_t and I_d. The coupling or even conflicting effects of forming parameters on each defect exist because of the different causing mechanisms, i.e., wrinkling by excessive compressive stresses, thinning by tensile stresses, and flattening by resultant forces along the cross-section of bent tubes. The dual indexes ($R_{d\,min}/D$, φ_{max}), i.e., the minimum $R_{d\,min}/D$, and the maximum bending angle, φ, are defined to fully identify the bending limits. It is known that the smaller R_d/D results

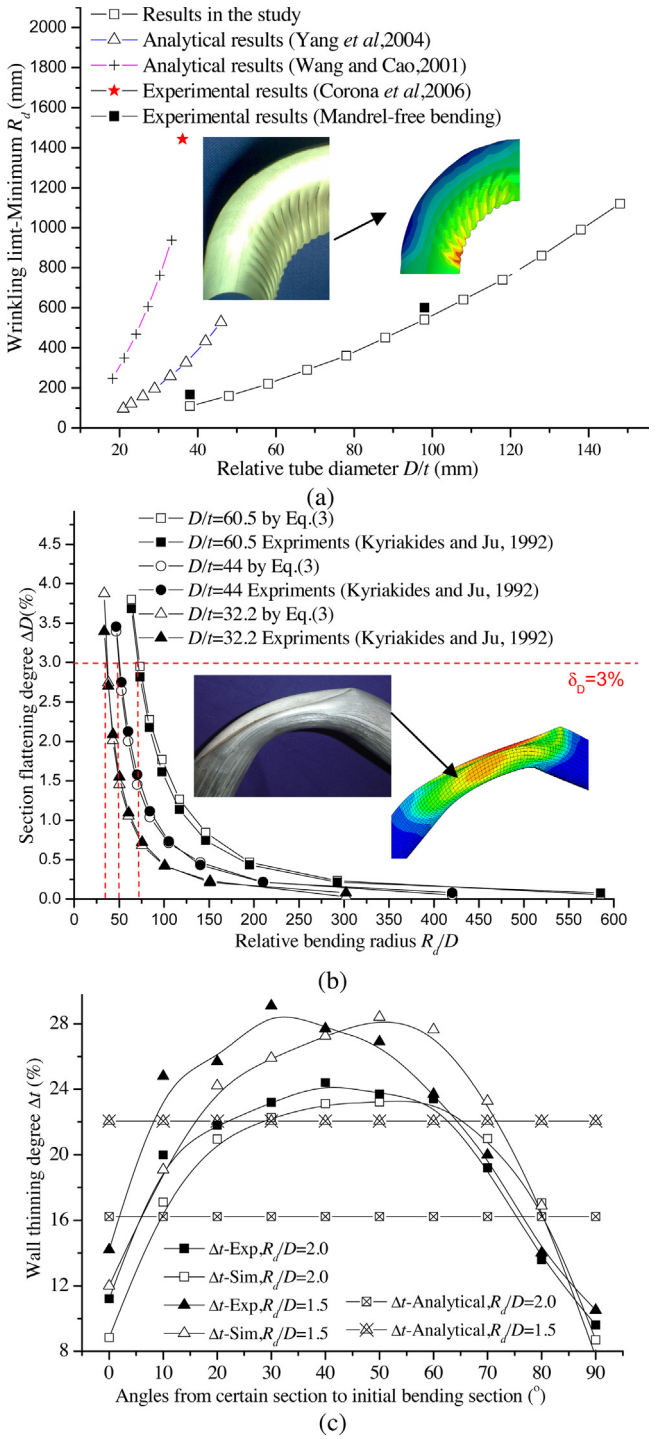

Fig. 5. Comparison of theoretical predictions with those of experiments and previous literature: (a) wrinkling limit; (b) flattening; (c) thinning.

in a higher wrinkling risk, more severe thinning and flattening. For bending angles, the wrinkling risk remains fairly constant at later bending stages, while both I_t and I_D increase significantly with increases in φ due to the unequal deformation at the extrados and intrados of bent tubes. Since the φ_{max} should be searched after the determination of $R_{d\,min}/D$, only the $R_{d\,min}/D$ is focused in the following sections. The detailed information is in supplementary file.

$$\frac{R_{d\,min}}{D, \varphi_{max}} = \phi(I_w, I_t, I_d) \quad (6)$$

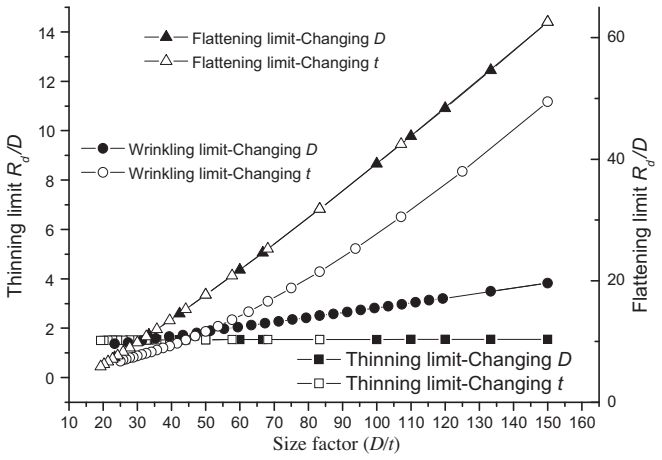

Fig. 6. Geometry-dependent bending limits.

$$\begin{cases} I_w = f(m, D/t, R_d/D, \varphi, T, f, c) \le \delta_w \\ I_t = f'(m, D/t, R_d/D, \varphi, T, f, c) \le \delta_t \\ I_d = f''(m, D/t, R_d/D, \varphi, T, f, c)\delta_d \end{cases}$$

where the material properties, m, include the hardening exponent, n, the strength coefficient, K, the normal anisotropic exponent, R, and the yield strength, $\sigma_{0.2}$. Tooling parameters, T, refer to the tooling sets, the mandrel diameter, and the mandrel extension length. The processing parameters f and c refer to the friction and the clearance between the tube and the tools. For discussion convenience, without special clarification, the tolerance for wrinkling, δ_w, is 0% (no visible wrinkle), that for thinning, δ_t, is 25%, and that for flattening, δ_D, is 5%.

3.2. Intrinsic factors dependent bending limits

3.2.1. Geometry-dependent tube bending limits

Fig. 6 shows the analytical predictions of the tube bending limits for all three instabilities. The wrinkling limit decreases with increasing D/t since larger D and smaller t both indicate a higher risk of wrinkling. The decreasing gradient of the wrinkling limit by decreasing t is greater than the decreasing gradient by increasing D. With respect to the thinning limit, the bending limit decreases slightly with larger values of D/t, and the effect of changing D is almost the same as the effect of changing t. The analyses show that the effect of D/t on the thinning limit is negligible. The reason is that the total incremental maximum of σ_φ at the tube extrados is only 2.5 MPa with D/t varying from 20 to 160 mm. Similar to the case with the wrinkling limit, the flattening limit decreases significantly with increasing D/t since larger D and smaller t cause weaker section rigidity. While the effect of D is similar to the effect of t. It is noted that the effect of D/t on the flattening limit is greater than its effect on the wrinkling limit.

From the energy point of view, for difficult bending conditions with large D and small t, the mandrel bending is required to avoid the onset of wrinkling, i.e., a wiper die or a mandrel with multiple flexible balls should be applied to exert dissipation energy, W', to reduce I_w as shown in Eq. (7). Then, the effects of D and t on the thinning limit and the flattening limit during mandrel bending are explored with the tube specifications shown in Table 4. The clearance between the mandrel shank and the tube, C_m, is determined for wrinkle-free bending. Initially, for bending with the largest D or smallest t, the maximum C_m for no wrinkling is determined. Then, it is assumed that C_m is a function of t, as shown in Eq. (8), where k' is a constant. Using Eq. (8), the C_m for other bending processes with

Table 4
Specification for geometry-dependent bending limit study.

Type	D (mm)	t (mm)
Changing D	19.05, 25.4, 31.75, 38.1, 44.45, 50.8	0.9
Changing t	50.8	0.5, 0.6, 0.7, 0.8, 0.9, 1.0
Same D/t (D/t = 56)	28, 33.6, 39.2, 44.8, 50.8, 56	0.5, 0.6, 0.7, 0.8, 0.9, 1.0

Table 5
Key forming parameters for the simulation of the geometry-dependent bending limit.

Forming parameters	Changing D	Changing t	Same D/t (D/t = 56)
Constant, k'	2/9	0.3	0.3
Mandrel extension length, e (mm)	5	5	3
Number of balls, N	4	4	3

no wrinkling is then determined. Following this strategy, a series of 3D-FE models are established with different tube geometrical parameters. Table 5 shows some key forming parameters. The tube is 6061-T4; the bending radius, R_d, equals 2.0D.

$$I_w = \frac{T}{W_{min}(W + W')} \tag{7}$$

$$C_m = k't \tag{8}$$

Fig. 7 shows that, during mandrel bending, Δt increases significantly with larger D/t, i.e., the maximum Δt reaches 7% with values of D/t ranging from 50 to 100 mm by decreasing t. This occurs because, with larger D/t, the tube should be closer to the bending tools to avoid wrinkling. However, this induces greater friction and thus greater tensile stresses, which could give rise to more severe thinning in extreme cases. For flattening, the opposite tendency is observed with larger D/t, i.e., the value of ΔD decreases with increasing D/t. This occurs because, under multiple-die constraints, ΔD is dominated by the mandrel parameters. With larger D/t, the clearance between the tube and the mandrel is smaller or constant to avoid wrinkling, as shown in Eq. (8), and thus, the value of ΔD decreases.

3.2.2. Material property-dependent bending limits

Table 6 shows the variations of tubular material properties, which covers a wide range of metallic tubular materials.

Fig. 8 shows the analytically calculated bending limits for the three instabilities under different material properties. For wrinkling limit, the hardening exponent, n, is the most significant

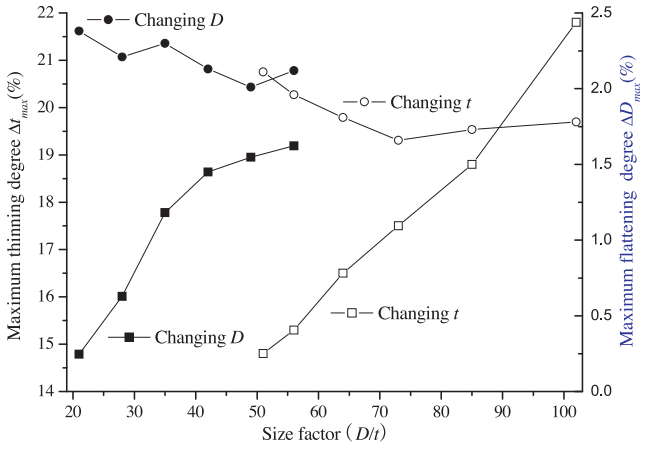

Fig. 7. Geometry-dependent bending limits under mandrel bending.

Table 6
The variations of tubular material properties.

Material properties	Values
Initial yield stress, $\sigma_{0.2}$ (MPa)	50, 90, 120, 150, 180, 210, 240, 270, 300, 340, 380, 420, 460, 500
Strength coefficient, K (MPa)	200, 300, 431, 600, 800, 1000, 1200, 1400, 1600
Strain hardening exponent, n	0.03, 0.05, 0.1, 0.15, 0.2, 0.262, 0.3, 0.35, 0.4, 0.45, 0.5, 0.55, 0.6
Normal anisotropy exponent, R	0.55, 0.6, 0.7, 0.8, 0.9, 1.0, 1.1, 1.2, 1.3, 1.3, 1.4, 1.5, 1.6, 1.7, 1.8, 1.9, 2.0

factor, and a larger n significantly improves the wrinkling-related bendability. A larger strength coefficient, K, and a normal anisotropic exponent, R, both result in slightly decreased wrinkling limits. For the thinning limit, the effect of n is similar to that on the wrinkling limit, and an increased R slightly improves the thinning limit. For the flattening limit, completely different effects are observed. The flattening limit decreases with increasing n and $\sigma_{0.2}$, and the flattening limit increases with increases in the strength coefficient, K.

Using 3D-FE models, the bending behaviors of a 5052-O tube are compared with those of a 1Cr18Ni9Ti tube. The bending specification is 38 mm × 1 mm × 57 mm. The clearance between the tube and the mandrel is 0.3 mm. Fig. 9 shows that wrinkling occurs for the Al-alloy tube, while stable deformation is achieved for the steel tube because of the significantly larger n of the stainless steel tube, as shown in Table 2. The wall thinning degree, Δt, of the steel tube is smaller than that of the Al-alloy tube, and the flattening degree,

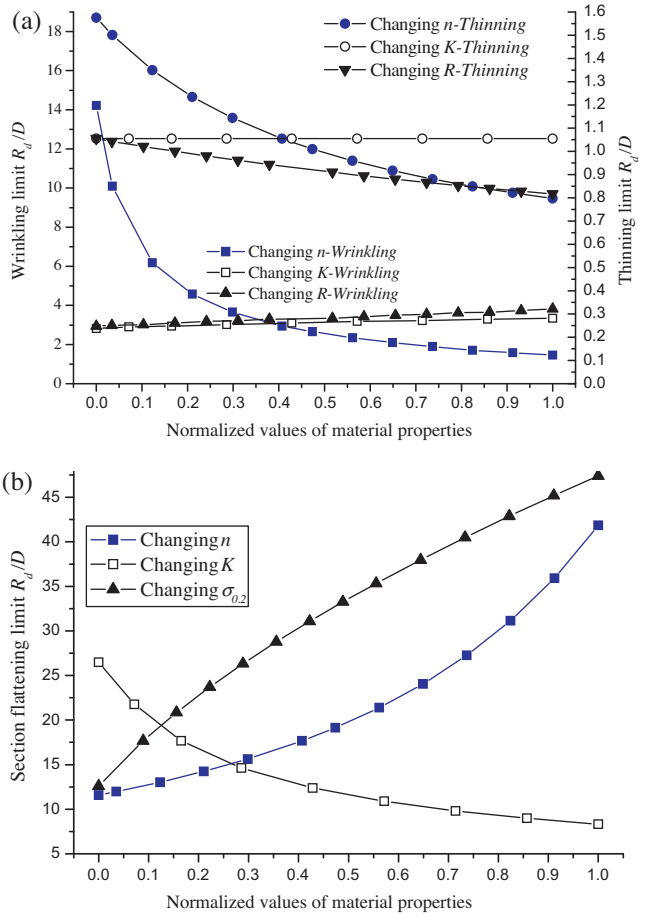

Fig. 8. Analytically obtained properties-dependent bending limits: (a) wrinkling limit and thinning limit; (b) flattening limit.

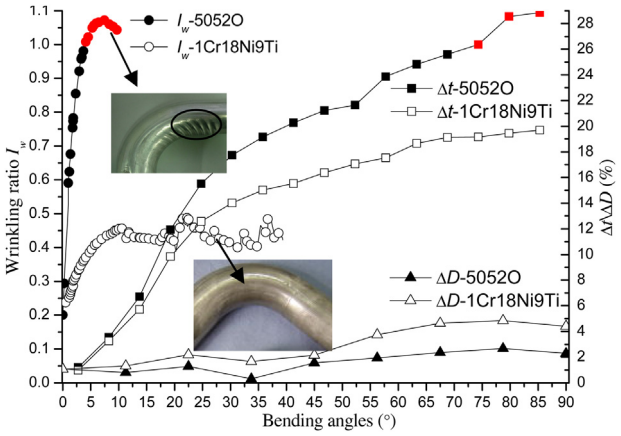

Fig. 9. Properties dependent bending limit under mandrel bending.

ΔD, of the 1Cr18Ni9Ti tube is larger than that of the 5052O tube. The analytically obtained obvious effects of the tube properties on the wrinkling limit and the flattening limit become less significant during mandrel bending. While, both analytical results and 3D-FE simulation show that the wall thinning is greatly affected by the material properties.

3.3. Effects of tooling/processing factors and uncertainties on bending limits

Given the basic design factors of D, t and m, the tube bendability can thus be evaluated, and then the appropriate tooling/processing parameters should be designed to improve the bending limits. As shown in Table 7, the coupling effects of the tooling/processing parameters on the multiple instability-constrained bending limits are verified.

- The push assistant speed, V_p/V, has little effect on the wrinkling limit, while both the thinning limit and the flattening limit are improved by the larger Vp/V.
- The mandrel plays the dominating role for bending limits. An increase in d can significantly reduce the risk of wrinkling, while Δt is increased, and ΔD is unaffected. With an increase in e, Δt increases, while ΔD decreases and the wrinkling is unaffected. An increase in the N enhances Δt, while both the wrinkling limit and the flattening limit are improved.

Table 7
Comparison of effects of tooling/processing parameters on multiple defects.

Forming parameters	Wrinkling risk	Thinning	Flattening
Push assistant speed, V_p/V↑	→	↓	↓
Mandrel↑			
Mandrel diameter d	↓↓	↑	→
Extension length e	→	↑	↓
Number of balls N	↓	↑	↓↓↓
Friction of tube-dies f↑			
Tube-mandrel f_m	↑	↑	↑
Tube-pressure die f_p	→	↓	↓
Tube-wiper die f_w	↓	↑	↑
Tube-bend die f_b	→	→	↓
Clearance of tube-dies c↑			
Tube-mandrel c_m	↑↑	↓	→
Tube-pressure die c_p	↑	↑	→
Tube-wiper die c_w	↑↑	↓	→
Tube-bend die c_b	→	→	→

Note: →-No effect; ↑-positive; ↓-negative; ↑↑-significantly positive; ↓↓-significantly negative; ↓↓↓-very significantly negative effect.
Tube-mandrel f_m means the contact interface between tube and mandrel.

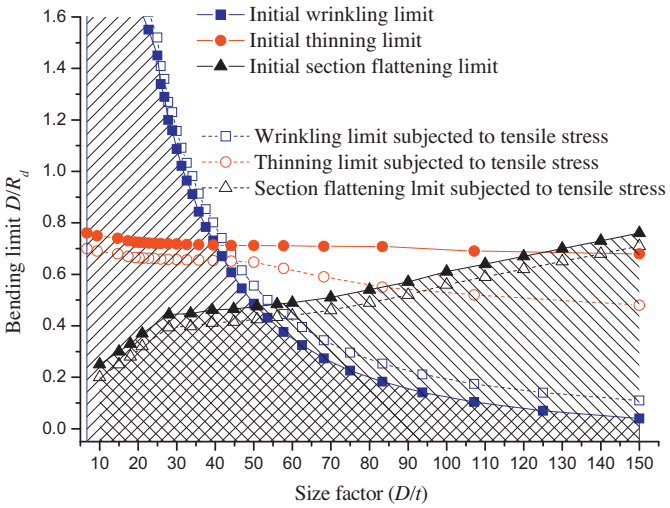

Fig. 10. Conceptual multiple defect-constrained BLD vs. basic design parameter D/t.

- The tool-tube friction directly changes the effect of the above tooling/processing factors on the bending limit (Oliveira et al., 2005). For instance, with increased f_m, a relative slip between the tube and the clamp die could be induced by the larger dragging force, causing the onset of wrinkling and aggravating Δt and ΔD. However, an increase in f_p results in a decrease in Δt and ΔD because of reduced tensile stress at the extrados of tube.
- The clearance between the tube and the tools greatly affect the wrinkling tendency and affects Δt and ΔD. For instance, the larger c_m, or c_w, may induce wrinkling, while Δt increases with smaller clearance.
- The major factors affecting Δt are c_p, f_p, c_m and f_m. In the case of wrinkling, the most significant tooling/processing factors are c_m, c_w, f_w and f_m. In the case of flattening, N, V_p/V, and e have the greatest influence.
- Due to multi-pass thermal-mechanical fabrication processes (SAE Aerospace, 2004), the properties and dimensions of the same brand of tube may vary to some extent. These uncertainties surely have obvious effects on bending quality of tubes. As an example, for a 6061-O tube of size 100 mm × 1.5 mm × 150 mm, the inner diameter variation of the tube significantly affects the wrinkling limit, and the wrinkling wave amplitude increases with larger tube inner diameter. In addition, the variation of inner tube diameter significantly affects thinning, but it has little effect on flattening.

3.4. Conceptual multiple defect-constrained bending limit diagram

The dependency of the intrinsic factors on the bendability lays the foundation for the optimal design of tooling/processing parameters for tube bending. Using the analytical models, regarding three instabilities, the basic design parameter-determined bendability can be evaluated by Eqs. (9)–(11). The controlling factors for each defect-related formability are different from each other.

$$F_w = \phi(D, t, R_d/D) \tag{9}$$

$$F_t = \phi(m, R_d/D, \varphi) \tag{10}$$

$$F_d = (D/t, R_d/D, \varphi) \tag{11}$$

Since D/t is the most vital parameter to be used for evaluating the bendability and optimally designing of tube bending, as shown in Fig. 10, the conceptual multiple defect-constrained bending limit

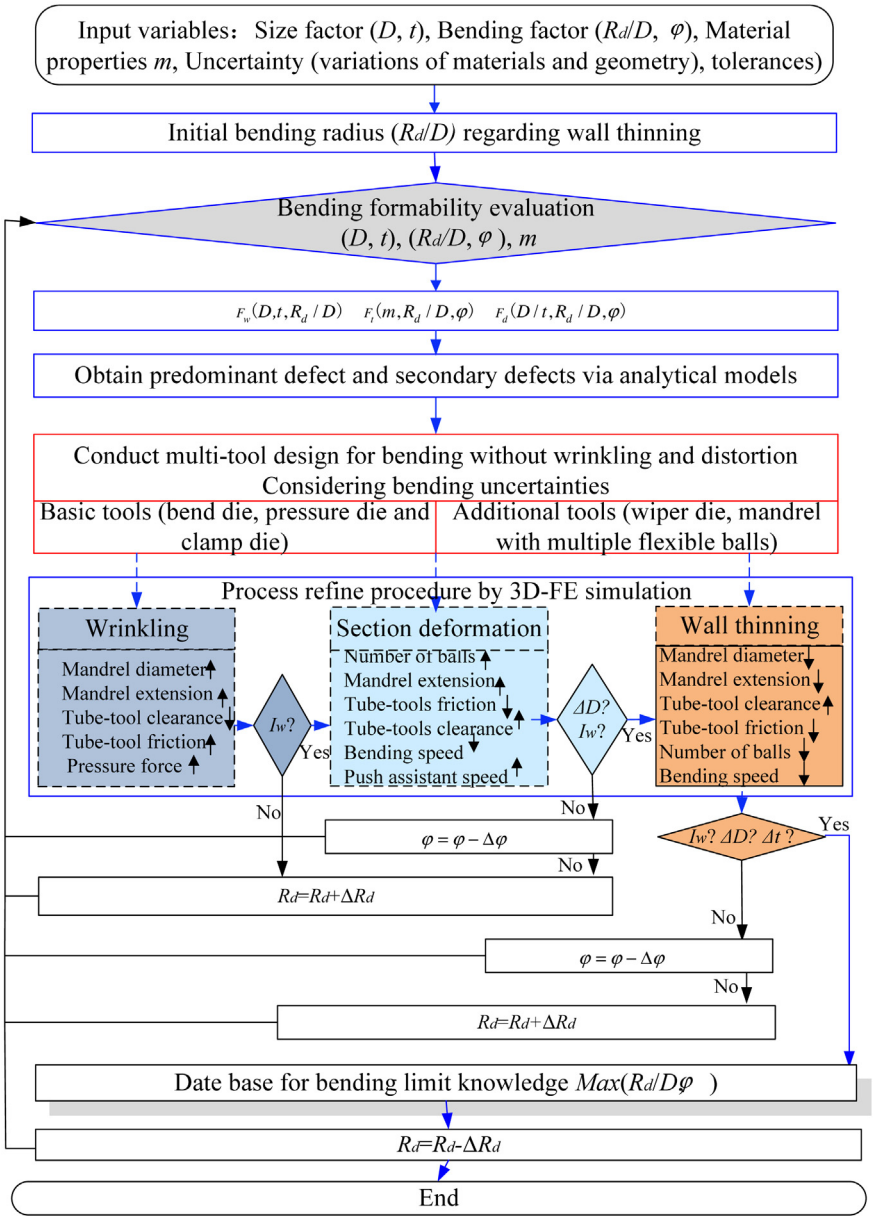

Fig. 11. Knowledge-based stepwise method for determining and improving bending limits.

is established with respect to D/R_d and D/t. The larger the D/R_d, the larger the bending limit is.

As shown in Fig. 10, there is a different dominant defect for bending with different tube geometrical parameters. Thus, different tooling/processing parameters should be deliberately selected. Because of the different causing mechanisms of the three instabilities, the conflicting effects of various parameters on multiple defects can be attributed to whether compressive stress or tension stress is induced. For instance, to avoid the wrinkling, the tensile stress is needed, while increasing tensile stress may cause severe Δt or ΔD.

3.5. *Stepwise method for determining and improving multiple defect-constrained limits*

The above analysis shows that the interactive effects or even conflicting effects on multiple defects make the design of tools/processing parameters a challenging issue. Thus, the intrinsic factor-dependent formability should be preliminarily obtained to identify which defect is the dominant instability as shown in Fig. 10, and then the tooling/processing parameters can be chosen based on the predominant defect. In this study, a knowledge-based stepwise method for determining and improving multiple instability-constrained bending limits of tubes is presented, as shown in Fig. 11.

- First, the bending formability is evaluated according to the basic parameters, i.e., the geometrical parameters of the tube (D, t), the bending factors $(R_d/D, \varphi)$ and the material properties, m. The predominant defect and secondary defects are obtained as shown in Eq. (9)–(11). Because the wall thinning is primarily determined by the material properties, the initial bending radius for the bending limit calculations can thus be obtained in this stage.
- Second, a suitable selection of multiple bending tools is conducted. The main concern is to avoid wrinkling or cross-section distortion by designing additional tools in addition to the basic tools because the wrinkling and cross-section flattening are dominated by the rigid supports of external and internal tools. Thus,

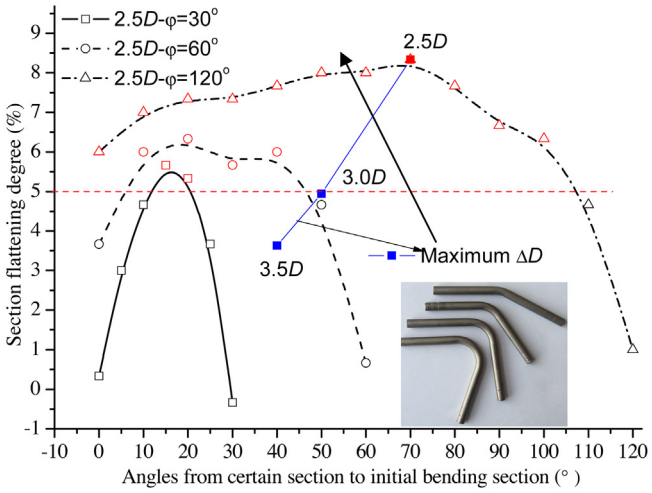

Fig. 12. Experimental results on flattening-constrained bending limit of Ti-tube, 6 mm × 0.6 mm.

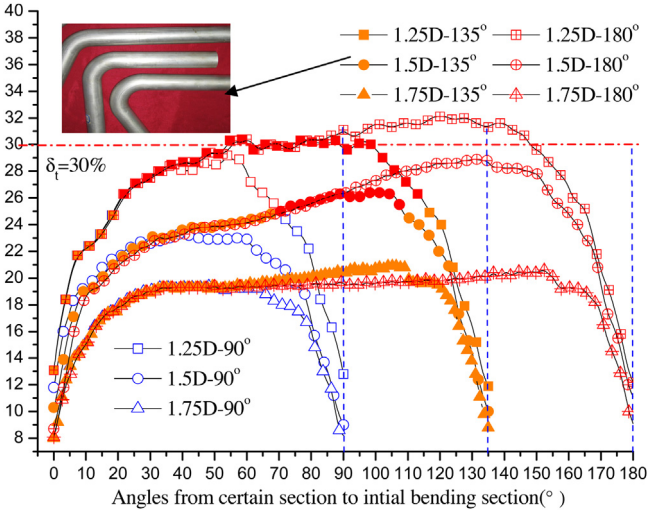

Fig. 13. Experimental results on bending limits of a thin-walled Al-alloy tube.

the tool selection for no wrinkling and allowable ΔD is ensured in this stage, in which the uncertainties should be considered.

- Third, according to the results of the bending formability, the tooling/processing parameters are further refined to overcome the major defect and secondary defects sequentially. The conflicting effects of the forming parameters on wrinkling, flattening and thinning must be considered. For each defect, the most significant factors should be designed or adjusted. Fig. 11 shows the detailed design sequence.
- Finally, according to the above sequential procedure, the database for the bending limit of tubes can be obtained, considering the three bending instabilities.

3.6. Case studies

3.6.1. Small diameter titanium alloy tubes

The bending limits of annealed Ti-3Al-2.5V titanium alloy tubes with small diameters, i.e., 6 mm × 0.6 mm and 14 mm × 1.35 mm, are tested. This bent tubes are used in hydraulic systems in aircraft with the allowed δ_t of 25%, the allowed δ_w of 0%, and the allowed δ_d of 5%. The procedure for determining and improving the bending limits is described below.

- The formability is first evaluated with respect to the three defects. Because the size factor, D/t, is approximately 10, according to Fig. 10, the major defect is flattening. Considering the fracture elongation of 13%, the initial bending radius, R_d, is assigned a value of 3.5D. Complete bending tools should be applied to improve the bending quality. For the 6 mm × 0.6 mm tube, D is too small to manufacture the mandrel and the wiper die. Thus, for this specification, only the basic bending tools are used, i.e., mandrel-free bending. However, for the 14 mm × 1.35 mm tube, besides the basic tools, the wiper die and the mandrel without flexible balls can be added.
- By increasing the mandrel extension length and push assistant speed, the flattening degree ΔD of the 6 mm × 0.6 mm tubes under 3.5D and 3.0D satisfies the quality tolerance of 5%. However, as shown in Fig. 12, under 2.5D, ΔD exceeds 5% for three bending angles, 30°, 60° and 120°. The bending limit of the 6 mm × 0.6 mm Ti-alloy tube is (3.0D, 90°) with ΔD of 4.6% and Δt of 11.6%. For the 14 mm × 1.35 mm tube, under a R_d of 2.2D, ΔD is less than 5%, and Δt is 16.2%. Thus, the bending limit of the 14 mm × 1.35 mm Ti-alloy tube is (2.2D, 180°).

3.6.2. Thin-walled aluminum alloy tube

This case focuses on the bending limit of a thin-walled 5052-O tube with the specification of 50 mm × 1 mm. δ_t is 30%, δ_w is 2%D, and δ_d is 10%. The procedure for determining and improving the bending limit is as follows.

- According to Fig. 10, the major defects are wrinkling and thinning for the thin-walled Al-alloy tube with D/t of 50. Due to the fracture elongation of nearly 20%, the initial R_d should be 2.75D to avoid over thinning. To avoid wrinkling, both wiper die and mandrel die with multiple flexible balls are employed.
- Strict forming parameters are used to prevent wrinkling, i.e., the mandrel extension length is 6 mm, the values of the mandrel diameter and the ball diameter are 47.6 mm, and three balls are used. Under these forming conditions, wrinkling can be avoided even for difficult bending of 1.25D as shown in Fig. 13.
- While, considering the wall thinning tolerance of 25%, the bending limit of this type of thin-walled Al-alloy tube is (1.25D, 90°) as shown in Fig. 13. It is confirmed that, the flattening degree remains 5%, and not the dominant defect for thin-walled Al-alloy tubes.

3.6.3. Thin-walled larger diameter Al-alloy tube

The bending limit of a large diameter thin-walled 6061-O Al-alloy tube with the specification of 150 mm × 1.5 mm is examined. The quality tolerance is the same as that described in Section 3.6.2. The procedure for determining and improving the bending limit is as follows.

- According to Fig. 10, the wrinkling is the dominant defect because of the large tube size D/t (ratio of 100). Due to the fracture elongation of nearly 26%, the initial R_d should be 2.0D to avoid over-thinning. To avoid wrinkling, both the wiper die and mandrel die with multiple flexible balls are used.
- Fig. 14(a) shows that under the applied conditions with a bending radius of 1.75D, the wrinkling still cannot be prevented. Thus, the tube-mandrel clearance should be further reduced to exert more dissipation energy to inhibit wrinkling. With the smaller clearance, the bent tubes without wrinkling are achieved as shown in Fig. 14(b). Under this condition, Δt is less than 30%, and ΔD is far less 10%. Thus, for this thin-walled larger diameter Al-alloy tube, the bending limit is restrained mainly by wrinkling, and the bending limit is (1.75D, 180°).

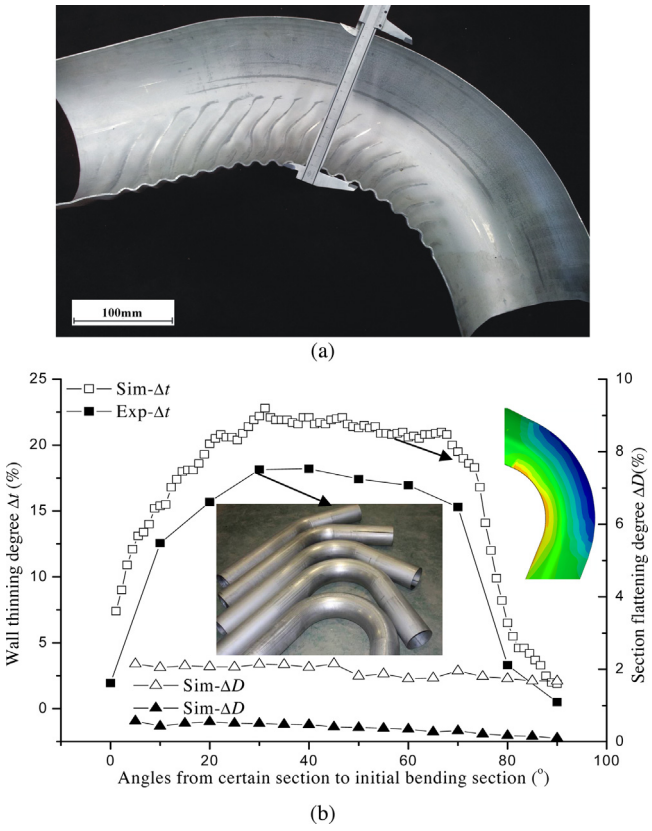

Fig. 14. Wrinkling-constrained bending limit of large diameter thin-walled Al-alloy tube 150 mm × 1.5 mm: (a) bent tubes with wrinkling; (b) qualified bent tubes without wrinkling.

4. Conclusions

Regarding wrinkling, thinning and flattening, a comprehensive map of the multiple defect-constrained forming limits of tubular material is addressed using theoretical and experimental methods. The main results are as follows.

(1) The dual indexes, minimum R_d/D and maximum φ are verified to consistently describe the multiple defect-constrained tube bending limits. The bending limit is the maximum among the wrinkling limit, thinning limit and flattening limit. The wrinkling limit changes little at later bending stages due to the incremental local bending characteristics of RDB.
(2) The intrinsic factor-dependent bending limits without considering contact conditions are addressed. A larger D/t implies a small wrinkling limit and a small flattening limit. The effect of D/t on the wrinkling limit and the flattening limit is far larger than its effect on the thinning limit, and the effect of t on wrinkling is larger than that of D. The hardening exponent has the largest effect on the three bending instabilities, and the conflicting effects are observed.
(3) Under mandrel bending, the intrinsic factor-dependent bending limits changes to some extent. The effects of D/t and m on the wrinkling limits are greatly weakened by the rigid support of bending tools, the neglected effects of D/t on the thinning limit are magnified, the significant influences of D/t on the flattening limit even become contrary, and the effects of m on wrinkling and thinning limit are opposite to that on the flattening limit.
(4) A conceptual multiple instability-constrained BLD (plotted vs. D/t) is developed, and a knowledge-based stepwise method for identifying and improving the tube bending limits is outlined considering coupling effects. The bending formability can be initially evaluated using basic design parameters, and then, tooling/processing parameters can be deliberately designed to coordinate the unequal deformation of the tube at the extrados and intrados. The method is verified by several practical bending scenarios for Ti-alloy tubes and Al-alloy tubes with extreme specifications.

Acknowledgements

The authors would like to thank the National Natural Science Foundation of China (50905144, 51275415), the Program for New Century Excellent Talents in University and 111 Project (B08040) for support for this research.

Appendix A. Supplementary data

Supplementary data associated with this article can be found, in the online version, at http://dx.doi.org/10.1016/j.jmatprotec.2013.09.027.

References

Corona, E., Lee, L.H., Kyriakides, S., 2006. Yield anisotropy effects on buckling of circular tubes under bending. Int. J. Solids Struct. 43, 7099–7118.
Goodarzi, M., kuboki, T., Murata, M., 2005. Deformation analysis for the shear bending process of circular tubes. J. Mater. Process. Technol. 162–163, 492–497.
Khodayari, G., 2008. Bending limit curve for rotary draw bending of tubular components in automotive hydroforming applications. SAE Int. J. Mater. Manuf. 1 (1), 841–848.
Kyriakides, S., Ju, G.T., 1992. Bifurcation and localization instabilities in cylindrical shells under bending-I. Experiments. Int. J. Solid Struct. 29 (9), 1117–1142.
Lee, J.W., Kwon, H.C., Rhee, M.H., Im, Y.T., 2003. Determination of forming limit of a structural aluminum tube in rubber pad bending. J. Mater. Process. Technol. 140, 487–493.
Lee, H., Tyne, C.J.V., Field, D., 2005. Finite element bending analysis of oval tubes using rotary draw bender for hydroforming applications. J. Mater. Process. Technol. 168, 327–335.
Li, H., Yang, H., Zhan, M., Gu, R.J., 2007a. The interactive effects of wrinkling and other defects in thin-walled tube NC bending process. J. Mater. Process. Technol. 187–188, 502–507.
Li, H., Yang, H., Zhan, M., Sun, Z.C., Gu, R.J., 2007b. Role of mandrel in NC precision bending process of thin-walled tube. Int. J. Mach. Tool Manuf. 47 (7–8), 1164–1175.
Li, H., Yang, H., Zhan, M., 2009. A study on plastic wrinkling in thin-walled tube bending via an energy-based wrinkling prediction model. Modell. Simul. Mater. Sci. Eng. 17 (3), 035007.
Mentella, A., Strano, M., 2012. Rotary draw bending of small diameter copper tubes: predicting the quality of the cross-section. Proc. IMechE Part B: J. Eng. Manuf. 226, 267–278.
Okude, Y., Sakaki, S., Yoshihara, S., Mac Donald, B.J., 2012. Increasing the working limit of extruded aluminum tubes during draw bending by introducing a wiper die. Mater. Trans. 53 (5), 875–878.
Oliveira, D.A., Worswick, M.J., Grantab, R., 2005. Effect of lubricant in mandrel-rotary draw tube bending of steel and aluminum. Can. Metall. Quart. 44, 71–78.
Paulsen, F., Welo, T., 2003. An analytical model for prediction of tube ovalization in bending. In: Brucato, Pr.V. (Ed.), The 6th International ESAFORM Conference on Material Forming (ESAFORM 2003). Salerno, Italy, pp. 775–778.
SAE Aerospace, 2004. Aircraft tube bending methods, techniques and tooling. Aerospace information repport. Air5378, issued 1999-12, Reaffirmed 2004-06.
SAE Aerospace, 2007. Tube bend radii. AS33611, issued 1997-8, Reaffirmed 2007-11.
Wang, X., Cao, J., 2001. Wrinkling limit in tube bending. J. Eng. Mater. Technol. (Trans ASME) 123 (4), 430–435.
Wu, W., Zhang, P., Zeng, X., Jin, L., Yao, S., Luo, A.A., 2008. Bendability of the wrought magnesium alloy AM30 tubes using a rotary draw bender? Mater. Sci. Eng. A 486 (1–2), 596–601.
Yang, H., Lin, Y., 2004. Wrinkling analysis for forming limit of tube bending processes. J. Mater. Process. Technol. 152, 363–369.
Yang, H., Li, H., Zhan, M., 2010. Friction role in bending behaviors of thin-walled tube in rotary-draw-bending under small bending radii. J. Mater. Process. Technol. 210, 2273–2284.
Zeng, Y.S., Li, Z.Q., 2002. Experimental research on the tube push-bending process. J. Mater. Process. Technol. 122, 237–240.